Inorganic Chemistry

Article

pubs.acs.org/IC

Series of Dicyanamide-Interlaced Assembly of Zinc-Schiff-Base Complexes: Crystal Structure and Photophysical and Thermal Studies

Monami Maiti,[†] Dipali Sadhukhan,[†] Santarupa Thakurta,[†] Syamantak Roy,[†] Guillaume Pilet,[‡] Ray J. Butcher,[§] Aline Nonat,[∥] Loïc J. Charbonnière,[∥] and Samiran Mitra*[,†]

[†]Department of Chemistry, Jadavpur University, Raja S. C. Mullick Road, Kolkata 700032, West Bengal, India

[‡]Groupe de Crystallographie et Ingénierie Moléculaire, Laboratoire des Multimatériaux et Interfaces, UMR 5615 CNRS-Université Claude Bernard Lyon 1, Bât. Chevreul, 43 bd du 11 Novembre 1918, 69622 Villeurbanne Cedex, France

[§]Department of Chemistry, Howard University, 2400 Sixth Street NW, Washington, DC 20059, United States

[∥]Laboratoire d'Ingénierie Moléculaire Appliquée à l'Analyse, IPHC, UMR 7178 CNRS/UdS, ECPM Bât R1N0, 25 rue Becquerel, 67087 Strasbourg Cedex 2, France

Supporting Information

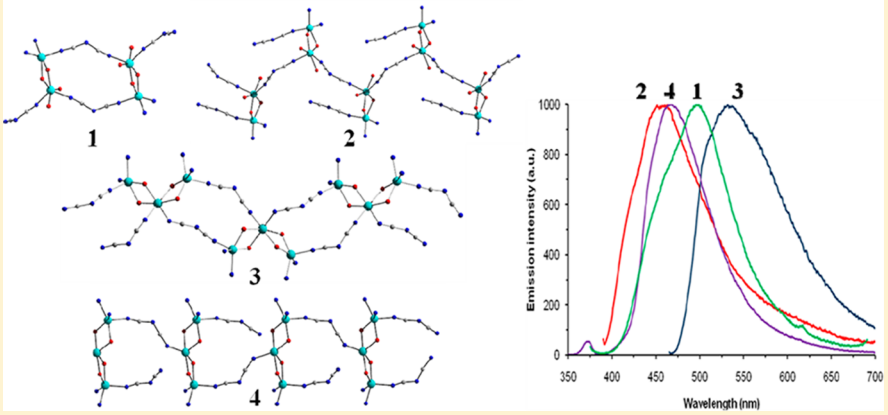

ABSTRACT: Four new dicyanamide (dca) bridged multinuclear Zn^{II}-Schiff-base complexes, $\{[Zn_2L^1(\mu_{1,5}\text{-dca})dca]\cdot CH_3OH\}_2$ (**1**), $[Zn_2L^2(\mu_{1,5}\text{-dca})dca]_n$ (**2**), $[Zn_3L^3{}_2(\mu_{1,5}\text{-dca})_2]_n$ (**3**), and $[(ZnL^4)_2Zn(\mu_{1,5}\text{-dca})dca]_n$ (**4**), have been synthesized using four different Schiff bases L^1H_2 = *N*,*N*′-bis(3-methoxysalicylidenimino)-1,3-diaminopentane, L^2H_2 = *N*,*N*′-bis(5-bromo-3-methoxysalicylidenimino)-1,3-diaminopropane, L^3H_2 = *N*,*N*′-bis(5-bromosalicylidenimino)-1,3-diaminopropane, and L^4H_2 = *N*,*N*′-bis(5-chlorosalicylidenimino)-1,3-diaminopropane and $NaN(CN)_2$ in order to extend the metal−ligand assembly. The directional properties of linear *end-to-end* bridging dca ligands have resulted in different metal ion connectivities leading to unique variety of templates in each of the complexes. All the ligands and complexes have been characterized by microanalytical and spectroscopic techniques. The structures of the complexes have been conclusively determined by single crystal X-ray diffraction studies. Thermogravimetric analyses have been performed to investigate the thermal stability of the metal−organic frameworks. Finally, the photoluminescence properties of the complexes as well as their respective ligands have been investigated with a comparative approach.

INTRODUCTION

Zinc is an important transition metal in chemistry as well as in biology. It constructs the active site of many hydrolytic enzymes and acts as Lewis acid catalyst.[1,2] In addition, zinc is the second most abundant trace metal after iron in biological systems and is essential to all forms of life.[2−5] Its flexibility in adopting various coordination numbers (4, 5, and 6) with suitable geometries (tetrahedral, square pyramidal/trigonal bipyramidal, and octahedral) is very important criterion for designing a wide variety of metal−organic frameworks. Moreover, electroluminescent (EL) zinc complexes attract a special attention because of their high light emitting efficiency and possibility of easy tuning the luminescence properties by ligand substitution.[6,7] Since the development of organic light emitting diode (OLED) material Alq_3 (q: 8-hydroxyquinolinyl)[8] numerous efforts have been employed to enrich the chemistry of full color RGB devices by designing green, blue, and red luminescent complexes. Zinc complexes of salicylaldimino Schiff bases are found to be promising materials to serve this purpose.[9,10] This particular type of Schiff bases has close resemblance to 8-hydroxyquinoline with respect to conjugation and chromophoric groups and is expected to promote luminescence properties of the Zn^{II} complexes which actually

Received: June 19, 2012
Published: October 31, 2012

 © 2012 American Chemical Society dx.doi.org/10.1021/ic3012958 | *Inorg. Chem.* 2012, 51, 12176−12187

Scheme 1. Synthetic Routes of the Schiff Base Ligands

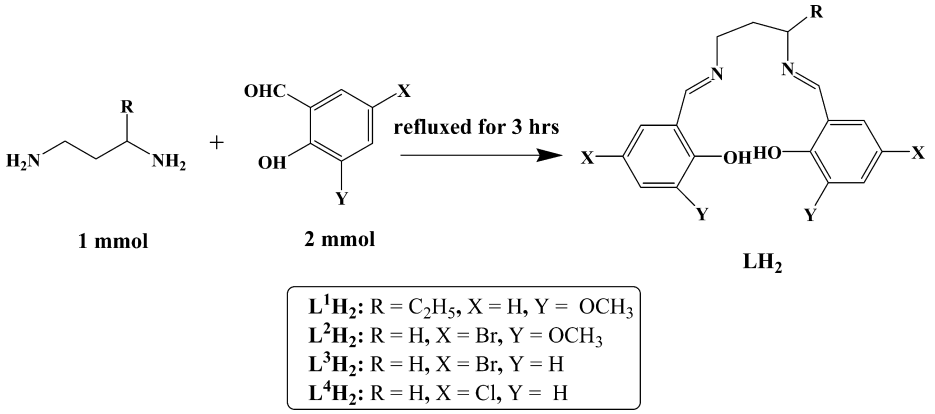

Scheme 2. Different Coordination Modes of Dicyanamide Ligand

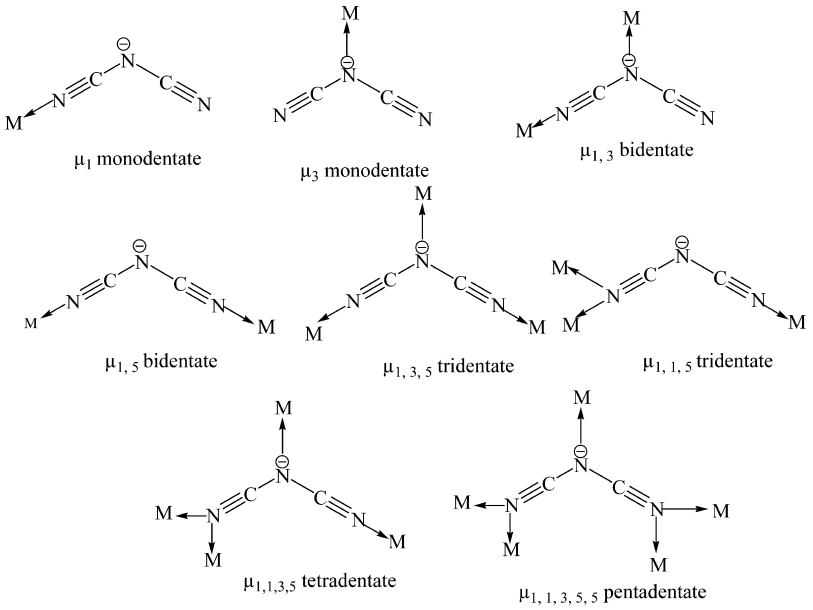

originates from the ligand centered excited states rather than LMCT. The presence of electronically saturated Zn^{II} ion is necessary because it imposes conformational rigidity to the ligand and prevents energy loss *via* bond vibration and electron transfer processes,[11] whereas paramagnetic transition metals quench fluorescence by different electron/energy transfer mechanisms.[12,13] Our group has previously synthesized luminescent complexes of different salicylaldimino Schiff bases with zinc[11,14,15] as well as lanthanoids.[16] As part of our efforts of searching for new luminescent materials, we have designed some conjugated aromatic Schiff bases by the condensation of 1,3-diamines and a few substituted salicylaldehydes (Scheme 1) to investigate the effect of electron donating and withdrawing groups on their luminescence properties.

Dicyanamide (dca), $N(CN)_2^-$, is a very flexible pseudohalide ligand which bridges metal ions through various coordination modes such as $\mu_{1,3}$ and $\mu_{1,5}$ bidentate, $\mu_{1,3,5}$ and $\mu_{1,1,5}$ tridentate, $\mu_{1,1,3,5}$ tetradentate, and $\mu_{1,1,3,5,5}$ pentadentate fashions etc.[17−20] as depicted in Scheme 2. Thus, dicyanamide acts as template for designing large varieties of molecular architectures from discrete dinuclear to multidimensional (nD, n = 1−3) networks.[21] A series of binary compounds with general formula $[M^{II}(dca)_2]_n$ (M = Cu, Co, Ni or Mn), exhibiting 3-D rutile type structures, have been reported.[22] In order to elaborate the 3-D systems with general formula $[M(L)(dca)_2]$, ancillary ligands such as pyrazine, 4,4′-bipyridine, pyrimidine, 4-methylpyrimidine, and 2,2′-bipyrimidine have been used in addition to dca ligand.[23] The network topologies are restricted to 2D or 1D in case of ternary systems $[M(dca)_2L_2]_n$, where L = imidazole, pyridine (or its substituted derivatives), chelating ligands like 1,10-phenanthroline, 2,2′-bipyridine, and several Schiff bases.[24−36] The terminal coordination of dicyanamide is not a common phenomenon due to the long chain length of the anion and charge delocalization over the symmetrical molecule. A search in the Cambridge Structural Database (CSD) revealed the record of 698 molecules with dca ligand. 223 of those (32%) contain a terminal dca ligand coordinated through one of the nitrile groups.[37] In our present case, a rare combination of the terminal as well as the $\mu_{1,5}$-bridging mode of dca enabled the design of unprecedented polymeric frameworks.

This Article primarily focuses on the synthesis and X-ray single crystal structure analyses of polymeric Zn^{II}-Schiff-base complexes, with the molecular architectures being designed by the flexibility and directional variations of dca chains. The thermal stabilities of the complexes have been examined by

dx.doi.org/10.1021/ic3012958 | Inorg. Chem. 2012, 51, 12176−12187

TGA. The physicochemical properties of four Zn^{II} complexes in comparison to respective Schiff bases have thoroughly been investigated.

EXPERIMENTAL SECTION

Materials. All chemicals and solvents employed for the syntheses were of analytical grade and used as received without further purification. 5-Bromosalicylaldehyde, 5-chlorosalicylaldehyde, *o*-vanillin (i.e., 2-hydroxy-3-methoxybenzaldehyde), 5-bromo-*o*-vanillin (i.e., 5-bromo-2-hydroxy-3-methoxybenzaldehyde), 1,3-propylenediamine (i.e., 1,3-diaminopropane) and ethyl propyl diamine (i.e., 1,3-diaminopentane), sodium dicyanamide, and zinc nitrate hexahydrate were purchased from Aldrich Chemical Co. Zinc trifluoroacetate was prepared by adding trifluoroacetic acid (E. Merck, India) to a paste of excess zinc carbonate (E. Merck, India) in water. The mixture was kept overnight for the completion of the reaction. It was then filtered and evaporated slowly on a steam bath till solidification and kept in a $CaCl_2$ desiccator for further use.

Syntheses of the Schiff Base Ligands [L^1H_2, L^2H_2, L^3H_2, and L^4H_2]. The synthetic route of the Schiff base ligands are depicted in Scheme 1.

The synthesis of *N*,*N*′-bis(3-methoxysalicylidenimino)-1,3-diaminopentane, L^1H_2, follows. L^1H_2 was obtained by the reflux condensation of 1,3-diaminopentane (10 mmol, 1.195 mL) with *o*-vanillin (20 mmol, 3.04 g) in 100 mL of methanol. The ligand was refluxed for 3 h resulting in a yellow solution. Vacuum evaporation of the resulting yellow solution gives the desired ligand in semisolid form. Yield 0.289 g (78%). Anal. Calcd (%) for $C_{21}H_{26}N_2O_4$ (M = 370.44 g/mol): C, 68.07; H, 7.08; N, 7.56. Found: C, 68.00; H, 7.02; N, 7.54. FT-IR bands (KBr, cm^{-1}): ν(C═N) 1629, ν(C−$O_{Phenolic}$) 1254, ν(O−H) 3449.

The synthesis of *N*,*N*′-bis(5-bromo-3-methoxysalicylidenimino)-1,3-diaminopropane, L^2H_2, follows. L^2H_2 was prepared following the same procedure as for L^1H_2 using 5-bromo-*o*-vanillin (20 mmol, 4.62 g) and 1,3-diaminopropane (10 mmol, 0.833 mL). The yellow crystalline ligand separated out upon cooling the solution and was collected by filtration and dried. Yield 0.45 g (90%). Anal. Calcd (%) for $C_{19}H_{20}Br_2N_2O_4$ (M = 500.18 g/mol): C, 45.62; H, 4.03; N, 5.60. Found: C, 45.72; H, 3.98; N, 5.70. FT-IR bands (KBr, cm^{-1}): ν(C═N) 1635, ν(C−$O_{Phenolic}$) 1260, ν(O−H) 3465.

The synthesis of *N*,*N*′-bis(5-bromosalicylidenimino)-1,3-diaminopropane, L^3H_2, follows. L^3H_2 was obtained by condensing 5-bromosalicylaldehyde (20 mmol, 4.02 g) with 1,3-diaminopropane (10 mmol, 0.833 mL) in 50 mL of methanol for 3 h. The crystalline ligand having a bright yellow color separated out upon cooling the solution which was collected by filtration. Yield 0.396 g (90%). Anal. Calcd (%) for $C_{17}H_{16}Br_2N_2O_2$ (M = 440.13 g/mol): C, 46.39; H, 3.66; N, 6.36. Found: C, 46.28; H, 3.59; N, 6.33. FT-IR bands (KBr, cm^{-1}): ν(C═N) 1633, ν(C−$O_{Phenolic}$) 1278, ν(O−H) 3535.

The synthesis of *N*,*N*′-bis(5-chlorosalicylidenimino)-1,3-diaminopropane, L^4H_2, follows. L^4H_2 was prepared following the same procedure as L^3H_2 with 5-chlorosalicylaldehyde (20 mmol, 3.13 g) as the carbonyl component. Slow evaporation of the resulting solution yielded shiny yellow crystalline Schiff base (L^4H_2). Yield 0.323 g (92%). Anal. Calcd (%) for $C_{17}H_{16}Cl_2N_2O_2$ (M = 351.23 g/mol): C, 58.13; H, 4.59; N, 7.98. Found: C, 58.09; H, 4.52; N, 7.92. FT-IR bands (KBr, cm^{-1}): ν(C═N) 1636, ν(C−$O_{Phenolic}$) 1278, ν(O−H) 3460.

Synthesis of {[$Zn_2L^1(\mu_{1,5}$-dca)dca]·CH_3OH}$_2$ (1). Zinc trifluoroacetate (0.291g, 1 mmol) was dissolved in 20 mL of 2-propanol. A methanolic solution of the Schiff base (L^1H_2) (0.370g, 1 mmol) was added to it followed by dropwise addition of aqueous solution of $NaN(CN)_2$ (0.195 g, 3 mmol). The mixture was allowed to stir for 40 min with gentle heating. The bright yellow solution was filtered and kept at 16 °C for crystallization. After two days light yellow block shaped single crystals suitable for X-ray crystallography were obtained. Yield 0.485 g (75%). Anal. Calcd (%) for $C_{25.5}H_{26}N_8O_{4.5}Zn_2$ (M = 647.30 g/mol): C, 47.29; H, 4.01; N, 17.31. Found: C, 47.27; H, 4.01; N, 17.30. FT-IR bands (KBr, cm^{-1}): ν(C═N) 1622, ν(C−$O_{Phenolic}$) 1171, ν(O−H) 3448, ν_{sym} + ν_{asym} (C≡N) 2357, 2345, ν_{asym} (C≡N) 2295, ν_{sym} (C≡N) 2223, ν(Zn−N) 454.

Synthesis of [$Zn_2L^2(\mu_{1,5}$-dca)dca]$_n$ (2). Compound **2** was prepared in a similar process as in the case of **1**, using 1 mmol of L^2H_2 (0.502 g) in methanol. Light yellow block shaped single crystals suitable for X-ray diffraction were obtained after three days. Crystals were isolated by filtration and were air-dried. Yield 1.248 g (82%). Anal. Calcd (%) for $C_{46}H_{36}Br_4N_{16}O_8Zn_4$ (M = 1522.03 g/mol): C, 36.27; H, 2.36; N, 14.71. Found: C, 36.31; H, 2.31; N, 14.75. FT-IR bands (KBr, cm^{-1}): ν(C═N) 1616, ν(C−$O_{Phenolic}$) 1234, ν_{sym} + ν_{asym} (C≡N) 2371, 2345, ν_{asym} (C≡N) 2244, ν_{sym} (C≡N) 2134, ν(Zn−N) 438.

Synthesis of [$Zn_3L^3{}_2(\mu_{1,5}$-dca)$_2$]$_n$ (3). $Zn(NO_3)_2{\cdot}6H_2O$ (0.893 g, 3 mmol) was dissolved in 20 mL of 2-propanol. A methanolic solution of the Schiff base (L^3H_2) (0.88 g, 2 mmol) was added to it followed by dropwise addition of aqueous solution of $NaN(CN)_2$ (0.178 g, 2 mmol). The solution was allowed to stir for 30 min at 25 °C. The final solution was kept at 16 °C yielding light yellow, block shaped single crystals suitable for X-ray diffraction. Yield 2.987 g (62%). Anal. Calcd (%) for $C_{152}H_{112}Br_{16}N_{40}O_{16}Zn_{12}$ (M = 4817.84 g/mol): C, 37.86; H, 2.32; N, 11.62. Found: C, 37.50; H, 2.67; N, 11.75. FT-IR bands (KBr, cm^{-1}): ν(C═N) 1627, ν(C−$O_{Phenolic}$) 1247, ν_{sym} + ν_{asym} (C≡N) 2379, 2360, ν_{asym} (C≡N) 2277, ν_{sym} (C≡N) 2213, ν(Zn−N) 456.

Synthesis of [(ZnL^4)$_2$Zn($\mu_{1,5}$-dca)dca]$_n$ (4). Compound **4** was prepared similarly as **3**, with the Schiff base ligand L^4H_2 (0.702 g, 2 mmol) in methanol. Light yellow block shaped single crystals suitable for X-ray diffraction were obtained on overnight standing at 16 °C. Crystals were isolated by filtration and were air-dried. Yield 0.739 g (72%). Anal. Calcd (%) for $C_{38}H_{28}Cl_4N_{10}O_4Zn_3$ (M = 1026.70 g/mol): C, 44.42; H, 2.73; N, 13.64. Found: C, 44.50; H, 2.77; N, 13.75. FT-IR bands (KBr, cm^{-1}): ν(C═N) 1629, ν(C−$O_{Phenolic}$) 1264, ν_{sym} + ν_{asym} (C≡N) 2372, 2313, ν_{asym} (C≡N) 2244, ν_{sym} (C≡N) 2177, ν(Zn−N) 473.

Physical Measurements. The Fourier transform infrared spectra were recorded in the range 4000−400 cm^{-1} on a Perkin-Elmer RX I FT-IR spectrophotometer with solid KBr pellets. C, H, and N microanalyses were carried out with a Perkin-Elmer 2400 II elemental analyzer. UV−vis absorption spectra were recorded on a Specord 205 (Analytik Jena) spectrometer. Steady state emission and excitation spectra were recorded on a Horiba Jobin Yvon Fluorolog 3 spectrometer working with a continuous 450W Xe lamp. For the measurement in the solid state, the spectrometer was fitted with a Quanta-Φ integrating sphere from Horiba. Detection was performed with a Hamamatsu R928 photomultiplier. All spectra were corrected for the instrumental functions. When necessary, a 399 nm cut off filter was used to eliminate the second order artifacts. The solid state luminescence quantum yield was determined using a Hamamatsu Quantaurus-QY integrating sphere according to the procedure described in refs 38a and 38b. The luminescence quantum yield Φ is given by

$$\Phi = \frac{E_i(\lambda) - (1 - A)E_0(\lambda)}{L_e(\lambda)A} \quad (1)$$

where

$$A = \frac{L_0(\lambda) - L_i(\lambda)}{L_0(\lambda)} \quad (2)$$

in which $E_i(\lambda)$ is the integrated luminescence of the film caused by direct excitation, $E_0(\lambda)$ is the integrated luminescence of the film caused by illumination from the sphere, A is the absorbance of the film, $L_e(\lambda)$ is the integrated excitation profile from the empty integration sphere (without the sample), $L_0(\lambda)$ is the integrated excitation profile when the sample is diffusively illuminated by the integration sphere, and $L_i(\lambda)$ is the integrated excitation profile upon direct excitation of the sample by the incident beam. The integrated spectra were corrected for the wavelength sensitivity of the photomultiplier and the spectral response of the sphere using correction functions furnished by the supplier.

dx.doi.org/10.1021/ic3012958 | Inorg. Chem. 2012, 51, 12176−12187

Table 1. Crystal Structure Parameters of the Complexes 1−4

param	complex **1**	complex **2**	complex **3**	complex **4**
empirical formula	$C_{25.50}H_{26}N_8O_{4.50}Zn_2$	$C_{46}H_{36}Br_4N_{16}O_8Zn_4$	$C_{152}H_{112}Br_{16}N_{40}O_{16}Zn_{12}$	$C_{38}H_{28}Cl_4N_{10}O_4Zn_3$
fw	647.30	1522.03	4817.84	1026.70
T	100 K	123 K	100 K	293 K
cryst syst	triclinic	monoclinic	orthorhombic	orthorhombic
space group	$P\bar{1}$	$C2/c$	$Fdd2$	$Pbcn$
a (Å)	8.9636(7)	17.4758(13)	32.349(5)	22.0584(4)
b (Å)	11.8050(11)	22.170(2)	27.916(5)	8.56486(19)
c (Å)	13.7543(12)	14.0515(11)	18.025(5)	21.1746(5)
α (deg)	94.286(7)	90	90	90
β (deg)	98.378(7)	97.660(8)	90	90
γ (deg)	106.098(8)	90	90	90
V (Å^3)	1373.2(2)	5395.3(8)	16 278(6)	4000.46(15)
Z	2	4	4	4
λ (Å)	0.71069	1.54178	0.71069	0.71069
d_{calc} (Mg m^{-3})	1.566	1.874	1.966	1.705
μ(mm^{-1})	1.796	6.058	5.736	2.107
F(000)	662	2992	9408	2064
θ range (deg)	3.4−29.6	3.24−75.66	3.4−29.7	1.8−29.3
total data	23 918	10 639	13 843	17 965
unique data	6840	5314	8196	4720
obsd data [$I > 2\sigma(I)$]	4862	5314	5436	3940
R1 [$I > 2\sigma(I)$]	0.0624	0.0674	0.0567	0.0442
wR2 [$I > 2\sigma(I)$]	0.0854	0.1740	0.0640	0.0480
S	1.08	1.064	1.041	1.083
R_{int}	0.048	0.0657	0.081	0.071
$\Delta\rho_{max}$ (e Å^{-3})	1.73	0.788	1.20	1.12
$\Delta\rho_{min}$ (e Å^{-3})	−1.04	−0.993	−1.47	−1.01

Luminescence quantum yields in solutions were determined on optically diluted samples (optical density < 0.05) according to eq 3[38c]

$$\Phi_x = \Phi_{ref} \times \left(\frac{n_x^2}{n_{ref}^2}\right) \times \left(\frac{\int I_{emx}(\lambda)\, d\lambda}{\int I_{emref}(\lambda)\, d\lambda}\right) \times \left(\frac{OD_{ref}}{OD_x}\right) \quad (3)$$

in which the subscripts x and ref refer, respectively, to the sample and the reference, n is the refractive index of the solution, $I_{em}(\lambda)$ is the emitted intensity at wavelength λ, and OD is the optical density of the sample. Thermogravimetric analyses of **1**−**4** were done in a Mettler Toledo TGA/SDTA 851 thermal analyzer.

Crystallographic Data Collection and Structure Refinements. The single crystals of compounds **1**−**4** were selected and mounted on an Oxford Diffraction Gemini diffractometer (**1**, **3**, and **4**) and on an Xcalibur Ruby Gemini diffractometer (**2**). Intensity data were collected using graphite-monochromatized Mo Kα radiation (λ = 0.710 69 Å) at 100 K for **1** and **3** and 293 K for **4**, and with Cu Kα radiation (λ = 1.541 78 Å) at 123 K for **2**. The structures of **1**, **3**, and **4** were solved by direct methods using the SIR97[39] program and refined by full-matrix least-squares methods with the program CRYSTALS.[40] Structure of **2** was solved by direct methods using the SHELXS 97 program[41] and refined by full-matrix least-squares methods using the SHELXL 97 program.[42] All the H atoms were generated geometrically and were included in the refinement by the riding model approximation. Selected crystallographic data, experimental conditions, and relevant features of the structural refinements for all complexes are summarized in Table 1.

RESULTS AND DISCUSSION

Crystal Structure of {[$Zn_2L^1(\mu_{1,5}$-dca)dca].CH_3OH}$_2$ (1). The perspective view of the asymmetric unit of the Zn^{II} complex (**1**) is shown in Figure 1, and the required bond lengths and angles are listed in Table 2. The asymmetric unit of **1** consists of a dinuclear core with two crystallographically independent zinc(II) ions, Zn1 and Zn2, linked together by a pair of phenoxo bridges of the Schiff base ligand $(L^1)^{2-}$. The distance between Zn1 and Zn2 is 3.163 Å and is within the range of the reported Zn···Zn separation in double phenoxo bridged Zn_2 complexes.[43,44] The pentacoordinated Zn1 ion is square pyramidal with Addison parameter τ = 0.1087 ($\tau = |\beta - \alpha|/60°$ where β and α are the two largest angles around the central atom; τ =0 for a perfect square pyramidal and 1 for a perfect trigonal bipyramidal geometry).[45] It occupies the N_2O_2 donor inner compartment of the Schiff base and is coordinated by the two imine nitrogens (N11 and N17) and the two

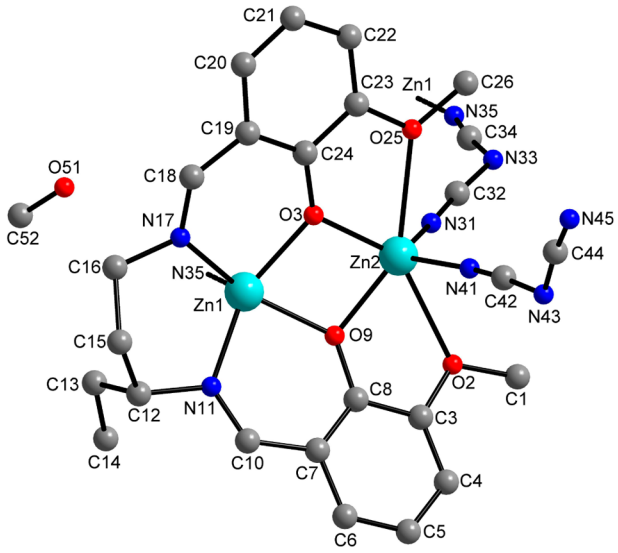

Figure 1. Perspective view of the asymmetric unit of complex **1**; H-atoms are not shown for clarity.

dx.doi.org/10.1021/ic3012958 | Inorg. Chem. 2012, 51, 12176−12187

Table 2. Selected Bond Lengths (Å) and Angles (deg) for Complex 1

Bond Lengths (Å)			
Zn1−O3	2.036(2)	Zn2−O3	2.004(3)
Zn1−O9	2.050(3)	Zn2−O9	2.002(3)
Zn1−N11	2.048(4)	Zn2−O25	2.526(3)
Zn1−N17	2.073(4)	Zn2−N31	1.963(3)
Zn1−N35	2.036(4)	Zn2−N41	1.966(4)
Zn2−O2	2.565(3)		
Bond Angles (deg)			
O3−Zn1−N11	148.31(12)	O2−Zn2−N31	78.56(12)
O3−Zn1−N17	88.14(14)	O2−Zn2−N41	82.22(13)
O3−Zn1−N35	101.53(13)	O3−Zn2−O9	77.63(11)
O3−Zn1−O9	75.81(10)	O3−Zn2−O25	68.47(9)
O9−Zn1−N11	88.37(12)	O3−Zn2−N31	118.92(13)
O9−Zn1−N17	154.83(14)	O3−Zn2−N41	111.93(14)
O9−Zn1−N35	97.05(13)	O9−Zn2−O25	145.96(10)
N11−Zn1−N17	95.87(14)	O9−Zn2−N31	117.86(12)
N11−Zn1−N35	107.61(13)	O9−Zn2−N41	110.10(13)
N17−Zn1−N35	105.19(16)	O25−Zn2−N31	77.93(12)
O2−Zn2−O3	145.09(9)	O25−Zn2−N41	86.10(13)
O2−Zn2−O9	67.48(9)	N31−Zn2−N41	114.96(15)
O2−Zn2−O25	146.23(8)		

phenoxo oxygens (O3 and O9) which form the basal plane of the square pyramid. The N35 end of a $\mu_{1,5}$-bridging dca nitrogen occupies the apical coordination site. Zn1 atom is 0.468 Å displaced toward apical N35 atom from the mean square plane passing through N11, N17, O3, and O9. The distorted octahedral Zn2 ion resides in the O_2O_2 donor outer compartment of $(L^1)^{2-}$. The equatorial plane around Zn2 is formed by the two μ-phenoxo oxygens (O3 and O9) and two methoxo oxygens (O2 and O25). The N31 end of a bridging dicyanamide ligand occupies one of the axial positions, and the other axial site is coordinated by the N41 end of a terminal dca ligand. Zn2 atom suffers *z*-in type Jahn−Teller distortion as the average axial bond distance (1.9645 Å) is smaller than the average equatorial bond distance (2.2742 Å). The average Zn−$O_{(methoxo)}$ linkages (2.5455 Å) are larger than the average Zn−$O_{(phenoxo)}$ linkages (2.003 Å). The steric hindrance caused by the methyl groups prevents the methoxo oxygens from approaching closer to Zn2 ion than the μ-phenoxo oxygens.

A pair of dimeric units form a centrosymmetric tetranuclear cluster, with the Zn1 ion of a unit being cooperatively connected to the Zn2 ion of the other by two $\mu_{1,5}$-dca ligands centered at N33 (Figure 2). Coexistence of $\mu_{1,5}$-bridging and nonbridging dicyanamide ligands is an important feature of the tetranuclear cluster. The free N end (N45) of the nonbridging dca participates in hydrogen bonding with the proton (H1) of a

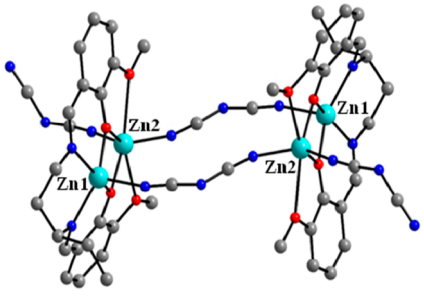

Figure 2. Centrosymmetric tetranuclear cluster of complex **1**.

lattice methanol molecule resulting in a strong O51−H1···N45 hydrogen bond with O51−N45 distance 2.893(7) Å and O51−H1···N45 bond angle ~180° (Figure S1 and Table S2). A weak C16−H162···O51 interaction is also perceptible between the methanolic oxygen O51 and azomethine carbon atom (C16) with C16−O51 distance of 3.346 Å and C16−H162···O51 angle of 136°. Adjacent tetranuclear molecules are interconnected by these centrosymmetric cooperative hydrogen bonding interactions assisted by the lattice methanol molecules and form a one-dimensional supramolecular chain along the crystallographic *c*-axis (Figure S1).

Crystal Structure of $[Zn_2L^2(\mu_{1,5}\text{-dca})dca]_n$ (2). The asymmetric unit of **2** is shown in Figure 3, and the bond

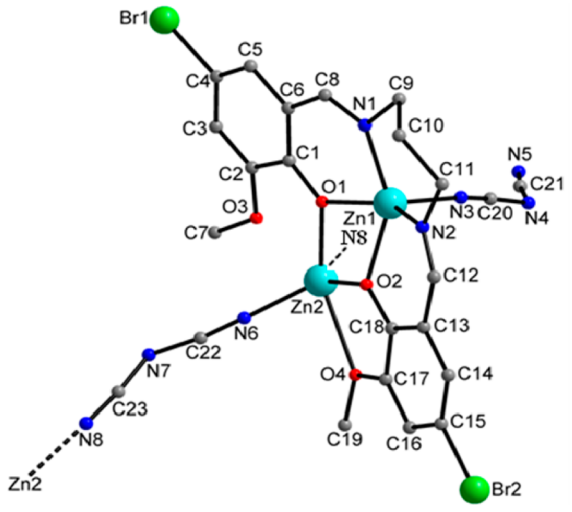

Figure 3. Perspective view of the asymmetric unit of complex **2**; H-atoms are not shown for clarity.

distances and angles around the metal centers are listed in Table 3. The dinuclear asymmetric unit of **2** is very similar to that of **1** with Zn1···Zn2 separation of 3.141 Å. Zn1 atom is square pyramidal (τ = 0.027)[45] but much less distorted than that in **1**. The N_2O_2 chromophore of $(L^2)^{2-}$ forms the basal plane, and the apical position is occupied by the N3 atom of a

Table 3. Selected Bond Lengths (Å) and Angles (deg) for Complex 2

Bond Lengths (Å)			
Zn1−O1	2.062(6)	Zn2−O1	2.013(7)
Zn1−O2	2.064(7)	Zn2−O2	1.990(6)
Zn1−N1	2.059(7)	Zn2−O4	2.458(6)
Zn1−N2	2.080(7)	Zn2−N6	1.954(8)
Zn1−N3	1.988(7)	Zn2−N8	1.965(8)
Bond Angles (deg)			
O1−Zn1−O2	74.8(2)	O1−Zn2−O2	77.5(2)
O1−Zn1−N1	87.1(3)	O1−Zn2−O4	147.7(2)
O1−Zn1−N2	149.4(3)	O1−Zn2−N6	117.6(3)
O1−Zn1−N3	102.0(3)	O1−Zn2−N8	107.8(3)
O2−Zn1−N1	147.8(3)	O2−Zn2−O4	70.4(2)
O2−Zn1−N2	86.5(2)	O2−Zn2−N6	117.6(3)
O2−Zn1−N3	101.7(3)	O2−Zn2−N8	113.5(3)
N1−Zn1−N2	97.1(3)	O4−Zn2−N6	81.5(3)
N1−Zn1−N3	108.0(3)	O4−Zn2−N8	82.6(3)
N2−Zn1−N3	105.4(3)	N6−Zn2−N8	116.5(4)

dx.doi.org/10.1021/ic3012958 | *Inorg. Chem.* 2012, 51, 12176−12187

pendant dca ligand. Unlike the octahedral Zn2 in **1**, the second metal center (Zn2) in **2** resides in a highly distorted square pyramidal environment tending toward trigonal bipyramidal geometry with τ = 0.5.[45] Two bridging phenoxo oxygens (O1 and O2), one methoxo oxygen (O4), and the nitrogen end (N6) of a $\mu_{1,5}$-bridging dca ligand form the basal plane around Zn2, and the apical position is occupied by the N8 end of another $\mu_{1,5}$-bridging dca ligand. The Zn2 atom is displaced by 0.606 Å from the basal plane formed by O1, O2, O4, and N6 toward the apical N8 atom.

The Zn2 centers of adjacent dinuclear units are interconnected by the N6 and N8 ends of $\mu_{1,5}$-dca single bridges resulting an infinite 1D zigzag polymeric pattern along the crystallographic *c* axis (Figure 4).

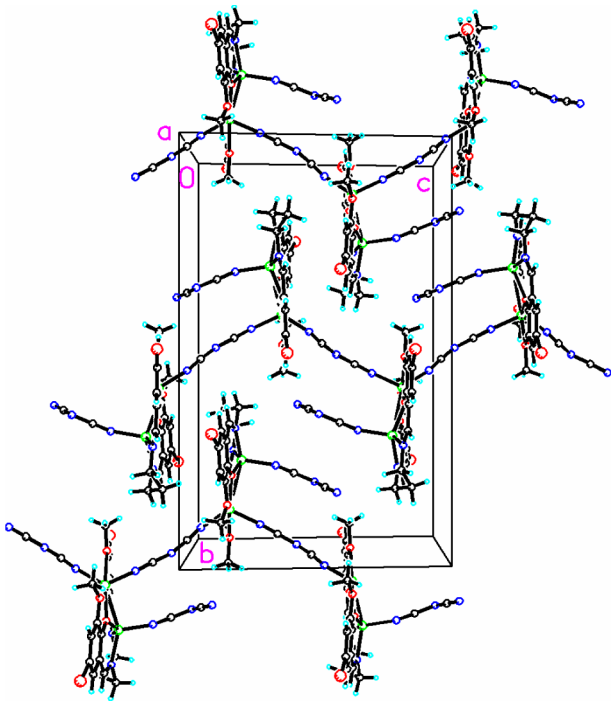

Figure 4. Crystal packing diagram of complex **2** showing the layers of single dca bridged zigzag 1D polymeric chain.

It is worth mentioning that, in both **1** and **2**, one of the two coordinated dca ligands is $\mu_{1,5}$-bridging while the other is nonbridging being pendant from Zn2 in **1** and from Zn1 in **2**. The presence of two bulky OMe groups in the aromatic rings of the Schiff base ligands eliminates the possibility of bridging of the pendant dca ligands. Only two dinuclear units are cooperatively connected by two $\mu_{1,5}$-dca having Zn1−Zn2 link in **1**, forming a discrete centrosymmetric tetranuclear cluster. The steric hindrance is more in **1** by the ethyl side chain that prevents further association of the molecules through dca chains unlike in **2** which forms an infinite 1D chain by interconnecting consecutive outer compartmental Zn2 atoms through single $\mu_{1,5}$-dca bridges.

Crystal Structure of $[Zn_3L^3{}_2(\mu_{1,5}\text{-dca})_2]_n$ (3). The asymmetric unit of **3** is shown in Figure 5, and the bond distances and angles around the metal centers are listed in Table 4. The asymmetric unit of **3** contains three crystallographically independent zinc ions (Zn1, Zn2, and Zn3) connected together by a pair of double phenoxo bridges of two Schiff base ligands $(L^3)^{2-}$ with Zn1−Zn2−Zn3 being held

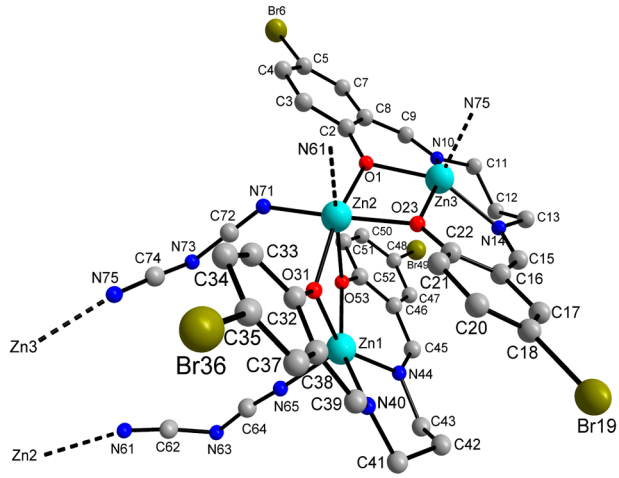

Figure 5. Perspective view of the asymmetric unit of complex **3**; H-atoms are not shown for clarity.

Table 4. Selected Bond Lengths (Å) and Angles (deg) for Complex 3

Bond Lengths (Å)			
Zn1−O31	2.054(8)	Zn2−O53	2.161(8)
Zn1−O53	2.025(7)	Zn2−N61	2.143(11)
Zn1−N40	2.096(11)	Zn2−N71	2.045(10)
Zn1−N44	2.119(11)	Zn3−O1	2.038(7)
Zn1−N65	2.005(11)	Zn3−O23	2.026(8)
Zn2−O1	2.118(8)	Zn3−N10	2.087(9)
Zn2−O23	2.051(7)	Zn3−N14	2.090(10)
Zn2−O31	2.135(9)	Zn3−N75	1.993(11)
Bond Angles (deg)			
O31−Zn1−O53	77.7(3)	O23−Zn2−N71	166.3(4)
O31−Zn1−N40	88.3(4)	O31−Zn2−O53	73.1(3)
O31−Zn1−N44	146.9(4)	O31−Zn2−N61	99.7(4)
O31−Zn1−N65	108.0(4)	O31−Zn2−N71	92.5(4)
O53−Zn1−N40	153.1(4)	O53−Zn2−N61	172.5(4)
O53−Zn1−N44	87.6(4)	O53−Zn2−N71	88.1(4)
O53−Zn1−N65	105.9(4)	N61−Zn2−N71	94.5(4)
N40−Zn1−N44	92.1(4)	O1−Zn3−O23	77.4(3)
N40−Zn1−N6	100.3(4)	O1−Zn3−N10	89.0(4)
N44−Zn1−N65	104.4(5)	O1−Zn3−N14	153.4(3)
O1−Zn2−O23	75.1(3)	O1−Zn3−N75	100.7(4)
O1−Zn2−O31	168.0(3)	O23−Zn3−N10	155.3(4)
O1−Zn2−O53	96.8(3)	O23−Zn3−N14	88.0(3)
O1−Zn2−N61	90.1(4)	O23−Zn3−N75	99.4(4)
O1−Zn2−N71	93.7(4)	N10−Zn3−N14	95.7(4)
O23−Zn2−O31	97.2(3)	N10−Zn3−N75	103.4(4)
O23−Zn2−O53	85.4(3)	N14−Zn3−N75	103.6(4)
O23−Zn2−N61	93.5(4)		

at an angle of 106.21(5)°. Two terminal zinc centers (Zn1 and Zn3) are chelated by the N_2O_2 chromophores of two ligands. Their geometry can be best described as a distorted 4 + 1(ONNO + N) square pyramid with Addison parameters τ = 0.103 and 0.032 for Zn1 and Zn3, respectively.[45] The square bases around Zn1 and Zn3 are formed by two imine nitrogen atoms and two phenolic oxygen atoms of the Schiff bases. The apical position is occupied by a nitrogen atom from the $\mu_{1,5}$-bridging dca ion. Zn1 is displaced from the mean plane constructed by N40, N44, O53, and O31 atoms by 0.520 Å toward the apical nitrogen atom (N65) where as Zn3 is displaced from the mean plane constructed by N10, N14, O23,

dx.doi.org/10.1021/ic3012958 | *Inorg. Chem.* 2012, 51, 12176−12187

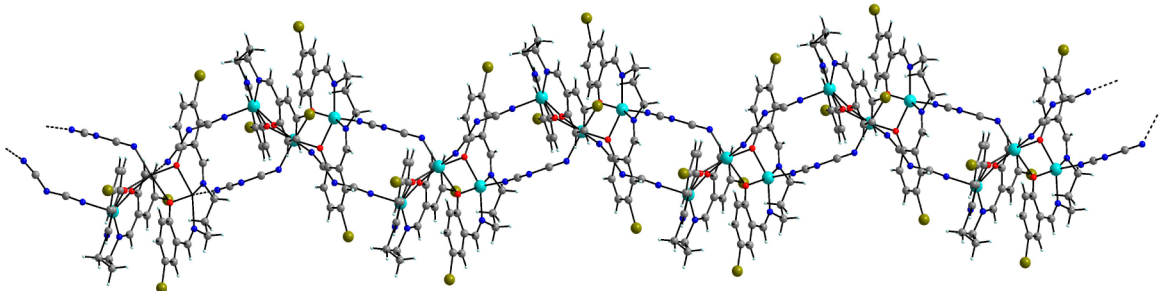

Figure 6. Double dca bridged looplike 1D polymeric chain of complex **3**.

and O1 by 0.426 Å toward the apical nitrogen atom (N75). The four bonds constituting the basal planes of Zn1 and Zn3 ions show very similar Zn−N and Zn−O bond distances (in the range 2.096(11)−2.025(7) Å for Zn1 and 2.087(9)-2.026(8) Å for Zn3).The apical Zn−N bond distances for both metal centers (Zn1−N65 = 2.005(11) Å and Zn3−N75 = 1.993(11) Å) resemble each other closely.

The central Zn2 ion occupies the octahedral hole formed by the four bridging phenoxo oxygens of two ligand units and two $\mu_{1,5}$-bridging dca ligands. The equatorial plane of the central Zn2 is constructed by three doubly bridging phenoxo oxygen atoms (O1, O23, and O31) of the Schiff base ligands $(L^3)^{2-}$ and a dca nitrogen atom (N71) while the axial positions of the octahedron are occupied by one bridging phenoxo oxygen atom (O53) and another dca nitrogen atom (N61). The 12 *cis*-angles (73.1(3)−99.7(4)°) and 3 *trans*-angles (166.3(4)−172.5(4)°) show significant deviations from ideal octahedral bond angles, and the average equatorial bond distances (2.087 Å) are smaller than the average axial bond distances (2.152 Å), indicating a *z*-out type tetragonal distortion from the ideal octahedral geometry.

All dca ligands are end-to-end bridging. The dca bridges are in the axial positions of Zn1 and Zn3 and bind cooperatively to Zn2 of two different neighboring moieties along the *c* axis (Figure 6). Thus, biphenoxo bridged Zn1−Zn2 and Zn2−Zn3 cores are pairwise connected to Zn2−Zn3 and Zn1−Zn2 moieties, respectively, of two neighboring units on either side of the crystallographic *c* axis resulting a 1D looplike coordination polymer.

Crystal Structure of $[(ZnL^4)_2Zn(\mu_{1,5}\text{-dca})dca]_n$ (4). The asymmetric unit of **4** (Figure 7) contains three zinc(II) ions, connected by a pair of double phenoxo bridges as observed in **3**. A C_2 axis passes through the central Zn1; hence, only two are the crystallographic independent Zn ions. The selected bond lengths and the bond angles are listed in Table 5. The Zn1−Zn2 distance (3.169 Å) is in agreement with that of complexes **1**−**3**. Terminal Zn^{II} center (Zn2) located at the inner N_2O_2 cavity of $(L^4)^{2-}$ is distorted square pyramidal (τ = 0.377)[45] as in **3** with very similar coordination core. Zn2 is displaced by 0.486 Å from the mean plane passing through N10, N14, O23, and O1atoms toward the apical nitrogen atom (N41) of the dca ligand.

Unlike in **3**, the central Zn1 in **4** describes a trigonal bipyramidal geometry [τ = 0.545][45] with large degree of distortion of the coordination polyhedron. Two bridging phenoxo oxygens (O1) and the $\mu_{1,5}$-bridging dca nitrogen atoms (N45) define the trigonal plane. The other two bridging phenoxo oxygens (O23) occupy the biaxial sites with O23−Zn1−O23_d angle 175.90(10)°. The axial Zn1−O23 bonds (2.134(2) Å) are slightly longer than the equatorial Zn1−O1 bonds (1.984(2) Å). The angles around Zn1 atom in the basal plane vary from 101.0(2)° to 143.2(2)° showing significant deviations from those bond angles (120°) in an ideal TBP polyhedron.

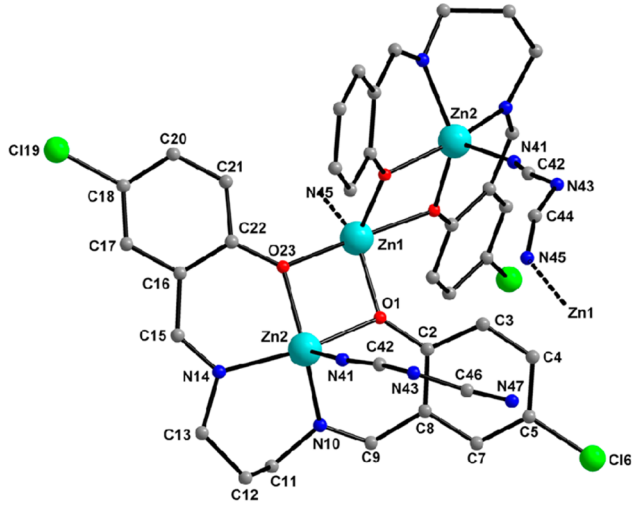

Figure 7. Perspective view of the asymmetric unit of complex **4**; H-atoms are not shown for clarity.

Table 5. Selected Bond Lengths (Å) and Angles (deg) for Complex 4[a]

Bond Lengths (Å)			
Zn1−O1	1.984(2)	Zn2−O1	2.077(2)
Zn1−O23	2.134(2)	Zn2−O23	1.994(2)
Zn1−N45_b	2.018(6)	Zn2−N10	2.057(3)
Zn1−O1_d	1.984(2)	Zn2−N14	2.070(2)
Zn1−O23_d	2.134(2)	Zn2−N41	2.034(3)
Bond Angles (deg)			
O1−Zn1−O23	77.63(8)	O1−Zn2−O23	78.78(8)
O1−Zn1−N45_b	101.0(2)	O1−Zn2−N10	86.20(9)
O1−Zn1−O1_d	115.37(10)	O1−Zn2−N14	162.59(10)
O1−Zn1−O23_d	100.14(8)	O1−Zn2−N41	93.89(12)
O23−Zn1−N45_b	81.7(2)	O23−Zn2−N10	140.17(10)
O1_d−Zn1-O23	100.14(8)	O23−Zn2−N14	91.40(9)
O23−Zn1−O23_d	175.90(10)	O23−Zn2−N41	111.04(12)
O1_d−Zn1−N45_b	143.2(2)	N10−Zn2−N14	92.51(10)
O23_d−Zn1−N45_b	102.2(2)	N10−Zn2−N41	106.58(12)
O1_d−Zn1−O23_d	77.63(8)	N14−Zn2−N41	103.09(12)

[a]Symmetry transformations used to generate equivalent atoms: b, *x*, 1 + *y*, *z*; d, 1 − *x*, *y*, $^3/_2$ − *z*. N45_e atom is identical to N45_b atom; the bond distance (Zn1−N45_e) and angles (X−Zn1-N45_e) have not been accounted in this table.

dx.doi.org/10.1021/ic3012958 | *Inorg. Chem.* 2012, 51, 12176−12187

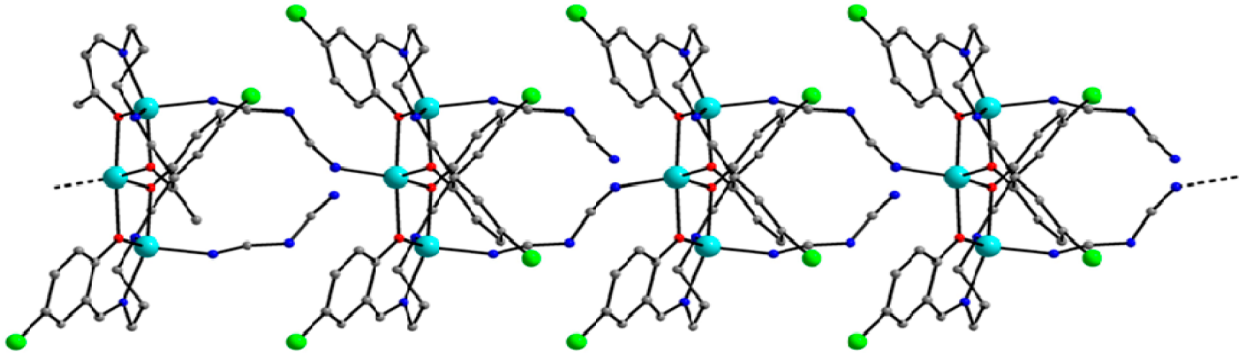

Figure 8. Single dca bridged zigzag 1D polymeric chain of complex **4**.

The dicyanamide ligand at the apical position of Zn2 is disordered over two positions (C44, N45 and C46, N47, respectively) with 50% site occupancy each. Consequently, one of the two symmetry equivalent Zn2 bound dca ligands bridges the central Zn1 atom of an adjacent molecule *via* N45 end, while the other dca (N47−C46−N43−C42−N41chain) is pendant from the second Zn2 atom with a free N47 end. Thus, adjacent trinuclear units are connected along the crystallographic *b* axis *via* single dca bridges with consequent Zn2−Zn1 connections resulting in an infinite 1D chain coordination polymer with a *zigzag* arrangement (Figure 8).

It is to be noted here that Br and Cl groups are introduced in the aromatic rings of the ligands of **3** and **4**, respectively. To avoid steric as well as electrostatic interaction due to the close proximity of halogen groups, the two halves of the molecules undergo conformational shift around the central Zn atom so that the halogens remain almost orthogonal. Such orthogonal orientation is accomplished by in plane and out of plane rotation of the two halves of the molecules in **3** and **4**, respectively. The situation allows a divergent orientation of the two dca ligands in **3** but a convergent orientation in **4**. Consequently, both dca ligands of a unit of **3** are capable of bridging two different metal ions of two adjacent trinuclear molecules on either direction of the crystallographic *c* axis, but only one of the two dca chains of a unit of **4** bridges a neighboring unit, the other being pendant on the same side along the crystallographic *b* axis. Thus, the trinuclear units are propagated by doubly bridging $\mu_{1,5}$-dca leading to a looplike 1D polymeric pattern in **3** but by singly bridging $\mu_{1,5}$-dca in **4** resulting in an zigzag 1D chain having a pendant dca from each unit quite similar to **2**. Packing forces also are not to be excluded in the formation of the observed topologies of the complexes.

Photoluminescence Studies. *Absorption Properties of the Ligands and the Complexes in EtOH.* The UV−vis absorption spectra of the Schiff-base ligands L^1H_2, L^2H_2, L^3H_2, and L^4H_2 were recorded at room temperature in EtOH (Figure S2). All spectra exhibit two distinct absorption bands at *ca.* 330 nm and *ca.* 420 nm (Table 6). These absorption bands can be assigned to $\pi \rightarrow \pi^*$ transitions of the Schiff-base ligands. A similar absorption spectrum has been reported for the *N*,*N*′-bis(salicylidene)-1,3-diaminopentane (L^0H_2).[14] The introductions of electron-withdrawing (Cl or Br) or electron-donating (OMe) groups both result in a 15−20 nm bathochromic shift of the absorption bands, and these effects are cumulative, with the introduction of both Br and OMe in L^2H_2 resulting in a supplementary shift of the maxima to low energy. Interestingly, electron-withdrawing substituents have a strong hyperchromic effect on the high energy absorption band. In contrast, the introduction of the methoxy group resulted in a decrease of the molar absorption coefficient for this transition. In L^2H_2 combining both donating and withdrawing groups, the effects are almost counterbalanced. It is surmised that the corresponding absorption bands imply electronic transitions centered on the phenolic moiety, the acido-basic properties of which are strongly influenced by the introduction of donating or withdrawing groups. Finally, all spectra exhibited a more or less pronounced shoulder at high energy (275 to 300 nm).

Table 6. Photophysical Properties of the Ligands in Absolute EtOH Solutions at Room Temperature

ligand	absorption λ_{ab}/nm (ε/M^{-1} cm^{-1})	excitation λ_{ex}/nm	emission λ_{em}/nm	quantum yield[a] Φ
L^0H_2	314 (5980), 401 (1720)	355	445	9.3×10^{-3}
L^1H_2	264 (11 350), 330 (2380), 421 (1110)	356	472	4.7×10^{-3}
L^2H_2	294 (7310), 339 (4350), 429 (3850)	368	514	7.0×10^{-3}
L^3H_2	279 (2840), 329 (7360), 416 (1240)	365	446	7.7×10^{-3}
L^4H_2	279 (2840), 329 (8100), 417 (1170)	365	448	6.4×10^{-3}

[a]In EtOH.

Although it was clear that the dissolution of the complexes (**1**−**4**) would result in a disruption of the chainlike structures observed in the solid state, we examined the UV−vis absorption spectra of the complexes in EtOH (Figure 9) to get insights into the influence of the Zn complexation on the absorption properties of the ligands. In all cases, the complexation resulted in a hypsochromic displacement of the lowest energy absorption band (Table S3). Despite the use of similar concentrations of the ligands and the complexes for all measurements, in the case of complex **4**, a doubling of the number of absorption band was observed, that was attributed to a partial decomplexation of the Zn cations.

Solution and Solid-State Luminescence Properties of the Ligands. Upon excitation in the UV domain (*ca.* 330 nm), the four ligands give rise to broad fluorescence above 400 nm. The excitation spectra of ligands L^1H_2, L^3H_2, and L^4H_2 are dominated by two intense bands centered at 275 nm and around 350−370 nm, respectively (Figure S3). As previously observed for other salicylidene derivatives,[14,16] the strong excitation band centered at *ca.* 360 nm does not correspond to any of the transitions recorded in the absorption spectra, and it was assigned to the emission of an excited state in the ketoamine form.[46−48] The excitation spectrum of ligand L^2H_2

dx.doi.org/10.1021/ic3012958 | *Inorg. Chem.* 2012, 51, 12176−12187

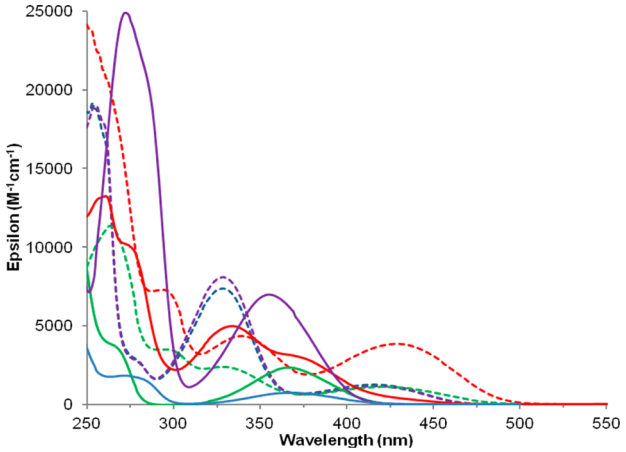

Figure 9. UV−vis absorption spectra of the complexes **1** (in purple), **2** (in blue), **3** (in green), and **4** (in red) in absolute EtOH at room temperature and of the corresponding ligands L^1H_2, L^2H_2, L^3H_2, and L^4H_2 (dotted lines).

significantly differs from the pattern previously observed for the other compounds of the series as it shows a much broader component in the red region, corresponding to the absorption band observed in the UV−vis absorption spectrum. The broad component around 430 nm, whose excitation spectrum is very similar to the absorption spectrum, probably arises from the emission of an excited state in the enolimine form (Figure S3).

Excitation at the maximum of the low energy excitation band resulted in the observation of broad emission bands with maxima at 472, 514, 446, and 448 nm, respectively, for L^1H_2 to L^4H_2 (Figure 10). The emission spectra recorded for L^3H_2 and

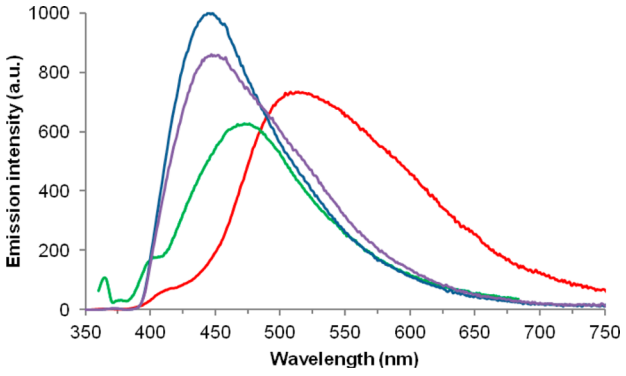

Figure 10. Fluorescence spectra of the ligands L^1H_2 (green, λ_{ex} = 356 nm), L^2H_2 (red, λ_{ex} = 368 nm), L^3H_2 (blue, λ_{ex} = 365 nm), and L^4H_2 (purple, λ_{ex} = 365 nm) in EtOH. All spectra were surface normalized according to their luminescence quantum yields.

L^4H_2 are very similar to the spectrum recorded for ligand L^0H_2,[14] whereas a 30 nm bathochromic shift is observed for ligand L^1H_2. The emission spectrum recorded for L^2H_2 is significantly broader than the one observed for the other ligands, as well as strongly red-shifted by 66 nm compared to L^4H_2. In the case of bromo substituted ligands L^2H_2 and L^3H_2, one can also notice shoulders on the low energy tail of the emission bands, which should arise from contribution of triplet state emission resulting from the heavy atom effect of the bromine atom.

The luminescence quantum yields of the ligands were determined in solution using optically diluted samples[38c] using ligand L^0H_2 as a reference ($\Phi = 9.3 \times 10^{-3}$ in MeOH),[14] and they amount to 4.7×10^{-3}, 7.0×10^{-3}, 7.7×10^{-3}, and 6.4×10^{-3}, respectively, for L^1H_2 to L^4H_2 (Table 6). These values indicate that the presence of a bromine or chlorine on the salicylidene skeleton induces a noticeable decrease of the quantum yields. Such behavior could be assigned to the heavy atom effect and suggests that L^2H_2, L^3H_2, and L^4H_2 might have a higher intersystem crossing (ISC) efficiency, resulting in a decrease of the emission from the singlet state due to population of the triplet state.[49−51]

As ligands L^2H_2, L^3H_2, and L^4H_2 have been isolated as powders, their luminescence properties have also been measured in the solid state (Figure 11). Upon excitation at

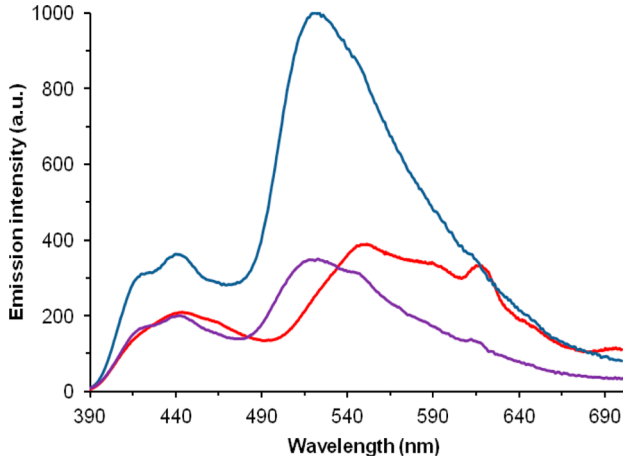

Figure 11. Normalized emission spectra of the ligands L^2H_2 (red, λ_{ex} = 368 nm), L^3H_2 (blue, λ_{ex} = 365 nm), and L^4H_2 (purple, λ_{ex} = 365 nm) in the solid state. All spectra were surface normalized according to their luminescence quantum yields.

ca. 365 nm, all three ligands display a smaller component centered around 440 nm and a stronger broad emission band centered at *ca.* 520−550 nm (the corresponding excitation spectra of L^2H_2, L^3H_2, and L^4H_2 can be found in Figure S4). These two components could be ascribed as arising from the emission of the singlet and the triplet excited states of the ligand, respectively, at 440 nm and 520−550 nm, in agreement with a strong intersystem crossing induced by the chloro, and more significantly, the bromo substituent. Interestingly, the maxima of emission are bathochromically shifted in comparison to those of the solution spectra. An 80 nm red shift is observed for ligands L^3H_2 and L^4H_2, whereas ligand L^2H_2 gives rise to a broader spectrum with the maximum of emission bathochromically shifted by 40 nm in comparison to the solution spectrum.

The luminescence quantum yields of the three ligands in the solid state have been measured with an absolute method based on the use of an integrating sphere and are very low resulting in large errors ($\pm 2 \times 10^{-3}$). Values of 3×10^{-3}, 4×10^{-3}, and 2×10^{-3} have been obtained for L^2H_2, L^3H_2, and L^4H_2, respectively.

Solid-State Luminescence Properties of the Zn^{II} Polymers. The photophysical properties of the coordination polymers of L^1H_2, L^2H_2, L^3H_2, and L^4H_2 with Zn^{II} (respectively **1**, **2**, **3**, and **4**) were examined in the solid state. Selected data are summarized in Table 7. Upon excitation at *ca.* 350 nm, the Zn(II) complexes display broad emission spectra with maxima at 474, 456, 534, and 467 nm for **1**, **2**, **3**, and **4**, respectively (Figure 12). Due to the different coordination polymers

dx.doi.org/10.1021/ic3012958 | *Inorg. Chem.* 2012, 51, 12176−12187

Table 7. Photophysical Properties of the Polymeric Zn(II) Coordination Complexes with Ligands L^1H_2, L^2H_2, L^3H_2, and L^4H_2 in the Solid State

complex	excitation (λ_{ex}/nm)	emission (λ_{em}/nm [Φ])
1	356	496 (<0.01)
2	368	456 (<0.01)
3	448	534 (0.072)
4	365	467 (0.027)

obtained with the four ligands, it is difficult to extract regular trends as might have been the case for isostructural polymers.

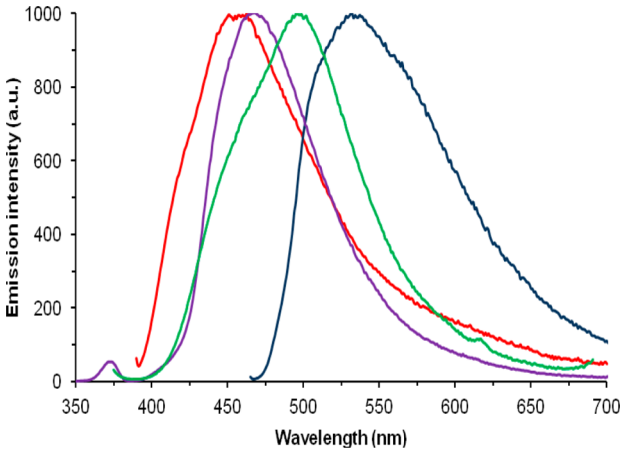

Figure 12. Emission spectra of **1** (green, λ_{exc} = 356 nm), **2** (red, λ_{exc} = 368 nm), **3** (blue, λ_{exc} = 448 nm), and **4** (purple, λ_{exc} = 365 nm), in the solid state (normalized to their maxima of emission).

For all complexes, only one component is observed in the emission spectra as described above (the corresponding excitation spectra of **1**–**4** are depicted in Figure S5). However, in the case of **1**, an intermediate emission spectrum centered at 496 nm is observed, which probably arises from both singlet and triplet excited states. Compound **2** gives rise to an emission from the singlet excited state centered at 456 nm which is 16 nm bathochromically shifted compared to the singlet state component of the emission band of L^2H_2 in solid state. However, the bromo derivative **3**, with a combination of electron deficient and heavy atom effect gives rise to red-shifted emission at 534 nm, which would correspond to phosphorescence from the triplet state of the ligand. The solid state emission spectrum of **4** is centered at 467 nm, which is around 20 nm bathochromatically shifted in comparison to the free ligand L^4H_2 in solution and is 27 nm bathochromically shifted with respect to the 440 nm component of solid L^4H_2 which corresponds to singlet state emission. Assuming that the two components observed in the ligand emission spectra in the solid state arise from the singlet and the triplet state, respectively, this would indicate that the emission observed for complex **4** as well as in complex **2** would mostly arise from the singlet state.

The luminescence quantum yields of the coordination polymers have been measured in the solid state, and results are summarized in Table 7. Overall quantum yields of 0.072 and 0.027 have been measured for **3** and **4**, respectively. These values are significantly higher than the one reported for other monometallic and dimetallic Zn^{II} complexes with salen-type Schiff base analogues.[14,52,53] Unfortunately, the quantum yields of the complexes with the methoxy derivatives **1** and **2** are too low to be determined accurately.

So, the ligand L^3H_2 and its polymeric Zn^{II} complex **3** have excellent luminescence properties in comparison to the other salicylidene derivatives, which probably arise from a strong intersystem crossing due to the presence of the electron withdrawing bromo substituent on the salicylidene skeleton. Low temperature measurements of the emission spectra and the luminescence lifetimes at 77 K would be necessary to further confirm this hypothesis but are out of the scope of the present study.

Thermogravimetric Analysis. The study of the thermal stability of the complexes is very important in order to use them as emissive materials. The thermal stabilities of complexes **1**–**4** have been investigated using TGA over a temperature range 25–800 °C in a single run in a dynamic nitrogen atmosphere.

Thermogravimetric studies of **1**–**4** indicated that the complexes are stable up to 510, 354, 234, and 305 °C, respectively. For **1**, the first stage of weight loss ~4.95% (calcd 4.94%) occurs in the temperature range 510–520 °C which corresponds to the loss of the lattice methanol molecule. On further heating the species decomposes in the range 520–535 °C corresponding to the elimination of the two dca ligands with a further mass loss of 20.40% (calcd 20.39%). For **2**, **3**, and **4** the first stage of mass loss occurs in the temperature range 354–375, 234–250, and 305–320 °C with a total mass loss of 8.03% (calcd 8.67%), 10.04% (calcd 10.96%), and 12.99% (calcd 12.86%) per formula unit, respectively, which corresponds to the loss of two dca moiety. No further mass loss was observed after the above-mentioned temperatures.

CONCLUSION

This paper describes the syntheses and structural aspects of the dicyanamide-bridged polymeric zinc complexes (**1**–**4**) with N_2O_4 or N_2O_2 donor Schiff base ligands. The nucleation of metal–ligand assembly in the complexes is controlled by the potential donor sites and the steric bulk of the Schiff bases. Packing forces also influence the formation of the observed topologies of the complexes. The dinuclear units of **1** and **2** encompass a rare combination of the terminal as well as end-to-end bridging dca and develop to a 1D supramolecular linear chain in **1** and a 1D zigzag molecular chain in **2**. In **3** and **4**, the respective divergent and convergent orientations of dicyanamide chains as well as the in plane and out of plane conformational shifts of the two halves of the molecules allow the chains to proliferate on either direction in **3** whereas the expansion is unidirectional in **4** along the procession axis. Thus, the trinuclear units are propagated by doubly bridging $\mu_{1,5}$-dca leading to looplike 1D polymeric pattern in **3** but by singly bridging $\mu_{1,5}$-dca in **4** resulting in a zigzag 1D chain having a pendant dca from each unit. Detailed photophysical investigations of the ligands and that of the complexes in solution as well as in solid state have been performed to search for the origin of emission. The experiment reveals that the ligands emit from both singlet and triplet excited states, and complexes **1**, **2**, and **4** are good fluorescent probes emitting from the singlet excited state whereas **3** undergoes ISC, influenced by electron withdrawing and the heavy atom effect of bromo substituent, and gives rise to phosphorescence. The complexes are thermally stable enough to be used as a potential luminescent probe.

dx.doi.org/10.1021/ic3012958 | *Inorg. Chem.* 2012, 51, 12176–12187

■ ASSOCIATED CONTENT

Supporting Information

Additional figures and tables. Crystallographic data in CIF format. This material is available free of charge via the Internet at http://pubs.acs.org. CCDC 874377, 874378, 874379, and 874380 contain the supplementary crystallographic data for **1**−**4**, respectively. These data can also be obtained free of charge from the Cambridge Crystallographic Data Centre via www.ccdc.cam.ac.uk/data_request/cif.

■ AUTHOR INFORMATION

Corresponding Author

*E-mail: smitra_2002@yahoo.com. Phone: +91 033 2414 6666 2779. Fax: +91 033 2414 6414.

Notes

The authors declare no competing financial interest.

■ ACKNOWLEDGMENTS

M.M. thanks UGC, and D.S. and S.M. thank CSIR [Project 01(2491)/11/EMR-II], New Delhi, Government of India, for financial support. We also thank Mr. Ashok Sasmal for some helpful discussions.

■ REFERENCES

(1) Lipscomb, W. N.; Sträter, N. *Chem. Rev.* **1996**, *96*, 2375−2433.
(2) Bertini, I.; Gray, H. B.; Lippard, S. J.; Valentine, J. S. *Bioinorganic Chemistry*; University Science Books: Mill Valley, CA, 1994.
(3) *Zinc in Human Biology*; Mills, C. F., Ed.; Springer-Verlag: New York, 1989.
(4) Vallee, B. L.; Auld, D. S. *Biochemistry* **1990**, *29*, 5647−5659.
(5) Prasad, A. S. *Biochemistry of Zinc*; Plenum: New York, 1993.
(6) Yang, W.; Schmider, H.; Wu, Q.; Zhang, Y.-S.; Wang, S. *Inorg. Chem.* **2000**, *39*, 2397−2404.
(7) He, J.; Yin, Y.-G.; Huang, X.-C.; Li, D. *Inorg. Chem. Commun.* **2006**, *9*, 205−207.
(8) Tang, C. W.; VanSlyke, S. A. *Appl. Phys. Lett.* **1987**, *51*, 913−915.
(9) Liuzzo, V.; Oberhauser, W.; Pucci, A. *Inorg. Chem. Commun.* **2010**, *13*, 686−688.
(10) Shi, Q.; Sheng, L.; Ma, K.; Sun, Y.; Cai, X.; Liu, R.; Wang, S. *Inorg. Chem. Commun.* **2009**, *12*, 255−258.
(11) Majumder, A.; Rosair, G. M.; Mallick, A.; Chattopadhyay, N.; Mitra, S. *Polyhedron* **2006**, *25*, 1753−1762.
(12) Zhao, P. S.; Wang, H. Y.; Song, J.; Lu, L. D. *Struct. Chem.* **2010**, *21*, 977−987.
(13) Dhara, K.; Karan, S.; Ratha, J.; Roy, P.; Chandra, G.; Manassero, M.; Mallik, B.; Banerjee, P. *Chem.—Asian J.* **2007**, *2*, 1091−1100.
(14) Sadhukhan, D.; Ray, A.; Rosair, G.; Charbonnière, L.; Mitra, S. *Bull. Chem. Soc. Jpn.* **2011**, *84*, 211−217.
(15) Sadhukhan, D.; Ray, A.; Pilet, G.; Rosair, G.; Garribba, E.; Mitra, S. *Bull. Chem. Soc. Jpn.* **2011**, *84*, 764−777.
(16) Chakraborty, J.; Thakurta, S.; Pilet, G.; Ziessel, R. F.; Charbonnière, L. J.; Mitra, S. *Eur. J. Inorg. Chem.* **2009**, 3993−4000.
(17) (a) Potoncak, I.; Dunaj, M.-J.; Miklos, D. M.; Jager, L. *Acta Crystallogr., Sect. C* **1996**, *52*, 1653−1655. (b) Potoncak, I.; Dunaj, M.-J.; Miklos, D. M.; Kabesova, M. *Acta Crystallogr., Sect. C* **1995**, *51*, 600−602.
(18) (a) Chow, Y. M. *Inorg. Chem.* **1971**, *10*, 1938−1942. (b) Chow, Y. M.; Britton, D. *Acta Crystallogr., Sect. C* **1977**, *33*, 697−699. (c) Manson, J. L.; Incarvito, C. D.; Rheingold, A. L.; Miller, J. S. *J. Chem. Soc., Dalton Trans.* **1998**, 2552−2560.
(19) Manson, J. L.; Kmety, C. R.; Huang, Q.; Lynn, J. W.; Bendele, G.; Pagola, S.; Stephens, P. W.; Liabe, L. M.-S.; Rheingold, A. L.; Epstein, A. J.; Miller, J. S. *Chem. Mater.* **1998**, *10*, 2552−2560.
(20) Chow, Y. M .; Britton, D. *Acta Crystallogr., Sect. C* **1975**, *31*, 1934−1937.
(21) (a) Martín., S.; Barandika, M. G.; Ruiz de Larramendi, J. I.; Cortés, R.; Font-Bardia, M.; Lezama, L.; Serna, Z. E.; Solans, X.; Rojo, T. *Inorg. Chem.* **2001**, *40*, 3687−3692. (b) Dalai, S.; Mukherjee, P. S.; Zangrando, E.; Ray Choudhuri, N. *New J. Chem.* **2002**, *26*, 1185−1189. (c) Riggio, I.; van Albada, G. A.; Ellis, D. D.; Spek, A. L.; Reedijk, J. *Inorg. Chim. Acta* **2001**, *313*, 120−124.
(22) (a) Batten, S. R.; Jensen, P.; Moubaraki, B.; Murray, K. S. *Chem. Commun.* **1998**, 439−440. (b) Kurmoo, M.; Kepert, C. J. *New J. Chem.* **1998**, *22*, 1515−1524.
(23) Escuer, A.; Mautner, F. A.; Sanz, N.; Vicente, R. *Inorg. Chim. Acta* **2002**, *340*, 163−169.
(24) (a) Batten, S. R.; Murray, K. S. *Coord. Chem. Rev.* **2003**, *246*, 103−130. (b) Miller, J. S.; Manson, J. L. *Acc. Chem. Res.* **2001**, *34*, 563−570.
(25) Manson, J. L.; Arif, A. M.; Incarvito, C. D.; Sands, L. M.-L.; Rheingold, A. L.; Miller, J. S. *J. Solid State Chem.* **1999**, *145*, 369−378.
(26) (a) Batten, S. R.; Jensen, P.; Kepert, C. J.; Kurmoo, M.; Moubaraki, B.; Murray, K. S.; Price, D. J. *J. Chem. Soc., Dalton Trans.* **1999**, 2987−2997. (b) Dasna, I.; Golhen, S.; Ouahab, L.; Pena, O.; Guillevic, J.; Fettouhi, M. *J. Chem. Soc., Dalton Trans.* **2000**, 129−132. (c) Albada van, G. A.; Castro, M. E.-Q; Mutikainen, I.; Turpeinen, U.; Reedijk, J. *Inorg. Chim. Acta* **2000**, *298*, 221−225. (d) Albada van, G. A.; Mutikainen, I.; Turpeinen, U.; Reedijk, J. *Acta Crystallogr., Sect. E* **2001**, *57*, m421−m423.
(27) Escuer, A.; Mautner, F. A.; Sanz, N.; Vicente, R. *Inorg, Chem.* **2000**, *39*, 1668−1673.
(28) (a) Dasna, I.; Golhen, S.; Ouahab, L.; Fettouhi, M.; Pena, O.; Daro, N.; Sutter, J. P. *Inorg. Chim. Acta* **2001**, *326*, 37−46. (b) Kou, H. Z.; He, Y. *Chem. Let.* **2003**, *32*, 902−903.
(29) Luo, J.; Hong, M.; Weng, J.; Zhao, Y.; Cao, R. *Inorg. Chim. Acta* **2002**, *329*, 59−65.
(30) Luo, J.-H.; Hong, M.-C.; Cao, R.; Liang, Y.-C.; Zhao, Y.-J.; Wang, R.-H.; Weng, J.-B. *Polyhedron* **2002**, *21*, 893−898.
(31) (a) Manson, J. L.; Incarvito, C. D.; Arif, A. M.; Rheingold, A. L.; Miller, J. S. *Mol. Cryst. Liq. Cryst. Technol., Sect. A* **1999**, *334*, 605−613. (b) Martin, S.; Barandica, M. G.; Larramendi de, J. I. R.; Cortes, R.; Font-Bardia, M.; Lezama, L.; Serna, Z. E.; Solans, X.; Rojo, T. *Inorg. Chem.* **2001**, *40*, 3687−3692.
(32) (a) Vangdal, B.; Carranza, J.; Lloret, F.; Julve, M.; Sletten, J. *J. Chem. Soc., Dalton Trans.* **2002**, 566−574. (b) Potocnak, I.; Burcak, M.; Wagner, C.; Jager, L. *Acta Crystallogr., Sect. C* **2002**, *58*, m327−m333. (c) Kooijman, H.; Spek, A. L.; Albada van, G. A.; Reedijk, J. *Acta Crystallogr., Sect. C* **2002**, *58*, m124−m126. (d) Wang, Z.-M.; Luo, J.; Sun, B.-W.; Yan, C.-H.; Gao, S.; Liao, C.-S. *Acta Crystallogr., Sect. C* **2000**, *56*, 786−788. (e) Carranza, J.; Brennan, C.; Sletten, J.; Lloret, F.; Julve, M. *J. Chem. Soc., Dalton Trans.* **2002**, 3164−3170.
(33) Sen, S.; Talukdar, P.; Rosair, G.; Yap, G.; Gramlich, V.; Kim, J.; Matsushita, T.; Desplanches, C.; Sutter, J.-P.; Mitra, S. *Inorg. Chim. Acta* **2005**, *358*, 2224−2230.
(34) Karmakar, R.; Choudhury, C. R.; Hughes, D. L.; Yap, G. P. A.; Fallah, M. S.; El Desplanches, C.; Sutter, J.-P.; Mitra, S. *Inorg. Chim. Acta* **2006**, *359*, 1184−1192.
(35) Banarjee, S.; Sen, S.; Basak, S.; Mitra, S.; Hughes, D. L.; Desplanches, C. *Inorg. Chim. Acta* **2008**, *361*, 2707−2714.
(36) Das, A.; Marschner, C.; Cano, J.; Baumgartner, J.; Ribas, J.; Salah El Fallah, M.; Mitra, S. *Polyhedron* **2009**, *28*, 2436−2442.
(37) Turner, D. R.; Chesman, A. S. R.; Murray, K. S.; Deacon, G. B.; Batten, S. R. *Chem. Commun.* **2011**, *47*, 10189−10210.
(38) (a) de Mello, J. C.; Wittmann, H. F.; Friend, R. H. *Adv. Mater.* **1997**, *9*, 230−232. (b) Pålson, L.-O.; Monkman, A. P. *Adv. Mater.* **2002**, *14*, 757−758. (c) Valeur, B. In *Molecular Fluorescence, Principles and Applications*, 5th ed.; Wiley-VCH: Weinheim, Germany, 2009; p 161.
(39) Altomare, A.; Burla, M. C.; Camalli, M.; Cascarano, G. L.; Giacovazzo, C.; Guagliardi, A.; Moliterni, A. G. G.; Polidori, G.; Spagna, R. *J. Appl. Crystallogr.* **1999**, *32*, 113−115.
(40) Watkin, D. J.; Prout, C. K.; Carruthers, J. R.; Betteridge, P. W. *CRYSTALS,*; Chemical Crystallography Laboratory: Oxford, U.K., 1999; Issue 11.

(41) Sheldrick, G. M. *Acta Crystallogr., Sect. A* **2008**, *64*, 112−122.
(42) Sheldrick, G. M. *SHELX-97*; University of Göttingen: Göttingen, Germany, 1997.
(43) Matalobos, J. S.; García-Deibe, A. M.; Fondo, M.; Navarro, D.; Bermejo, M. R. *Inorg. Chem. Commun.* **2004**, *7*, 311−314.
(44) Maxim, C.; Pasatoiu, T. D.; Kravtsov, V. Ch.; Shova, S.; Muryn, C. A.; Winpenny, R. E. P.; Tuna, F.; Andruh, M. *Inorg. Chim. Acta* **2008**, *361*, 3903−3911.
(45) Addison, A. W.; Rao, T. N.; Reedijk, J.; Rijn, J.; van.; Verschoor, G. C. *J. Chem. Soc., Dalton Trans.* **1984**, 1349−1356.
(46) Rofríguez-Santiago, L.; Sodupe, M.; Oliva, A.; Bertran, J. *J. Am. Chem. Soc.* **1999**, *121*, 8882−8890.
(47) Mitra, S.; Tamai, N. *Chem. Phys. Lett.* **1998**, *282*, 391−397.
(48) Catalan, J.; Toribio, F.; Acuña, A. U. *J. Phys. Chem.* **1982**, *86*, 303−306.
(49) Bolton, O.; Lee, K.; Kim, H.-J.; Lin, K. Y.; Kim, J. *Nat. Chem.* **2011**, 205−210.
(50) Saigusa, H.; Azumi, T. *J. Chem. Phys.* **1979**, *71*, 1408−1413.
(51) Hamanoue, K.; Nakayama, T.; Tsujimoto, I.; Miki, S.; Ushida, K. *J. Phys. Chem.* **1995**, *99*, 5802−5808.
(52) Lü, X.-Q.; Feng, W.-X.; Hui, Y.-N.; Wei, T. J.; Song, R.; Zhao, S.-S.; Wong, W.-Y.; Wong, W.-K.; Jones, R. A. *Eur. J. Inorg. Chem.* **2010**, 2714−2722.
(53) Bi, W.; Wei, T.; Lü, X.; Hui, Y.; Song, J.; Zhao, S.; Wong, W. -K.; Jones, R. A. *New J. Chem.* **2009**, *33*, 2326−233.